Optics Letters

Optically tunable Fano resonance in a grating-based Fabry–Perot cavity-coupled microring resonator on a silicon chip

WEIFENG ZHANG, WANGZHE LI, AND JIANPING YAO*

Microwave Photonic Research Laboratory, School of Electrical Engineering and Computer Science, University of Ottawa, 800 King Edward Avenue, Ottawa, Ontario K1N 6N5, Canada
**Corresponding author: jpyao@eecs.uottawa.ca*

Received 19 April 2016; accepted 22 April 2016; posted 26 April 2016 (Doc. ID 263548); published 19 May 2016

A grating-based Fabry–Perot (FP) cavity-coupled microring resonator on a silicon chip is reported to demonstrate an all-optically tunable Fano resonance. In the device, an add-drop microring resonator (MRR) is employed, and one of the two bus waveguides is replaced by an FP cavity consisting of two sidewall Bragg gratings. By choosing the parameters of the gratings, the resonant mode of the FP cavity is coupled to one of the resonant modes of the MRR. Due to the coupling between the resonant modes, a Fano resonance with an asymmetric line shape resulted. Measurement results show a Fano resonance with an extinction ratio of 22.54 dB, and a slope rate of 250.4 dB/nm is achieved. A further study of the effect of the coupling on the Fano resonance is performed numerically and experimentally. Thanks to the strong light-confinement capacity of the MRR and the FP cavity, a strong two-photon absorption induced nonlinear thermal-optic effect resulted, which is used to tune the Fano resonance optically.

OCIS codes: (130.3120) Integrated optics devices; (050.2770) Gratings; (230.5750) Resonators.

http://dx.doi.org/10.1364/OL.41.002474

Fano resonance, as opposed to a conventional Lorentz resonance with a symmetric line shape, has an asymmetric line shape, which resulted from the interference between a discrete localized state and a continuum state [1]. Thanks to the sharp asymmetric line shape, Fano resonance has been employed for applications such as high-sensitivity sensing [2] and low power optical switching and modulating [3,4]. Considerable work has been performed to achieve a sharp asymmetric Fano resonance theoretically and experimentally in a different material platform [5–7]. Due to its compatibility with the mature complementary metal–oxide–semiconductor (CMOS) fabrication technique, silicon photonics has attracted the worldwide attention for low cost, high volume, and reliable manufacturing of photonic devices with nanoscale precision and for potential integration with electrical devices [8]. Numerous silicon-based nanostructures have been proposed to exhibit a Fano resonance. For example, an integrated silicon Bragg reflector was demonstrated to produce a Fano resonance by interfering the light waves reflected from the Bragg grating and the end facet of the waveguide [9]. However, due to the low reflection efficiency of the end facet, the extinction ratio (ER) of the Fano resonance is as low as 3–4 dB and the slope rate (SR) is also as low as around 10 dB/nm, which are too small for applications where a Fano resonance with a very sharp line shape is required.

Thanks to their compact footprint and whispering-gallery resonator nature, microring resonators (MRRs) have been significantly investigated for numerous different applications. By the interference of two resonant beams in an MRR, a Fano resonance could be generated, and the shape of the Fano resonance could be tunable via controlling the phase difference between the two beams by a heater [10]. However, the system incorporated a multimode interference coupler (MMI) and a waveguide crossing, which largely increased the complexity of the device. The tunability is achieved using a heater, which inevitably increases the fabrication cost of the device. To reduce the system cost, particular interest is paid to generating the Fano resonance in a coupled waveguide-resonator system in which a waveguide, functioning as a resonator by the two facet reflection, is coupled to another resonator of a photonic crystal cavity or an MRR [11–15]. The first side-coupled waveguide resonator system was implemented by coupling a waveguide with partially reflecting elements to a photonic crystal cavity [11]. Based on this model, an ultra-compact resonant system was proposed to exhibit the asymmetric Fano resonance in which a waveguide Fabry–Perot (FP) resonator is laterally coupled to a tiny photonic crystal nanobeam cavity. A Fano resonance with an ER of 7.3 dB and an SR above 5 dB/nm was experimentally demonstrated. However, its low ER and SR imposes limitations on its widespread applications, since a very sharp asymmetric line shape of the Fano resonance can greatly reduce the required phase change for high-sensitivity sensing or low power optical switching/modulating. Therefore, it is highly preferred that a Fano resonance spectrum has a high ER and a large SR. In addition, as all-optical information processing and networking schemes are expected to overcome the speed limitations imposed of pure electronic

systems and fully exploit the long distance transmission capabilities offered by photonics [16], an all-optically tunable Fano resonance is of particular interest for all-optical integrated circuits. However, all-optically tunable Fano resonances on a silicon chip has, so far, never been demonstrated.

In this Letter, a grating-based FP cavity-coupled MRR on a silicon chip is reported to demonstrate an all-optically tunable Fano resonance. In the proposed device, an add-drop MRR is employed, and one of the two bus waveguides is replaced by an FP cavity consisting of two sidewall Bragg gratings as two reflectors, which are realized by introducing periodic corrugations in the bus waveguide sidewalls. By choosing the grating period and the cavity length, a resonant mode of the FP cavity is coupled to one of the resonant modes of the MRR. Due to the coupling between the resonant modes, a Fano resonance with an asymmetric line shape is generated. The proposed device is fabricated and experimentally evaluated. Measurement results show that a Fano resonance with an ER of 22.54 dB and an SR of 250.4 dB/nm is achieved. A further study of the effect of the coupling between the MRR and FP cavity on the Fano resonance is performed numerically and experimentally. Thanks to the strong light-confinement capacity of the MRR and the FP cavity, when a pumping light with a wavelength at a resonance wavelength of either the MRR or the FP cavity is fed into the device, a strong two-photon absorption (TPA)-induced nonlinear thermal-optic effect would be produced, which will affect the coupling between the MRR and the FP cavity. By varying the power of the pumping light, the Fano resonance is tuned. The experimental results show that a maximum tuning range of 90 pm is achieved, which could be increased by increasing the power of the pumping light or elevating the quality factor (Q-factor) of the resonators. To the best of our knowledge, this is the first time that a Fano resonance is tuned by using the TPA-induced nonlinear optical effect in silicon. The key advantage of the proposed device is that the incorporation of the FP cavity in the MRR can maintain the compactness of the MRR without increasing the complexity since the FP cavity is formed in one of the bus waveguides, and can, also, easily realize the all-optical tuning of the Fano resonance through optical pumping due to the high light-confining capacity of the resonators.

The waveguide consists of a thin silicon layer (220 nm thick) on top of a buried oxide layer (2 μm thick) on a silicon wafer. A strip waveguide with a width of 500 nm is employed as the fundamental waveguide structure. Figure 1(a) illustrates the perspective of the proposed grating-based FP cavity-coupled MRR. The device has an add-drop MRR configuration in which an FP cavity, consisting of two identical sidewall Bragg gratings as two reflectors, is used to replace one of the two bus waveguides. Thus, one side of the MRR is laterally coupled with the FP cavity and the other side is laterally coupled with a bus waveguide. Figure 1(b) shows the top view of the coupling region between the MRR and the FP cavity. The gratings are realized by introducing periodic corrugations to the sidewalls of the strip waveguide. To make the grating work at 1550 nm, the corrugation depth is chosen to be 35 nm and the grating period is designed to be 320 nm with a duty cycle of 50%. The FP cavity formed by the two gratings has a length of 4.72 μm, and each grating has a length of 64 μm. Figure 1(c) gives the cross-sectional view of the device along the direction from A to B on Fig. 1(a). The MRR has a diameter of 16.2 μm

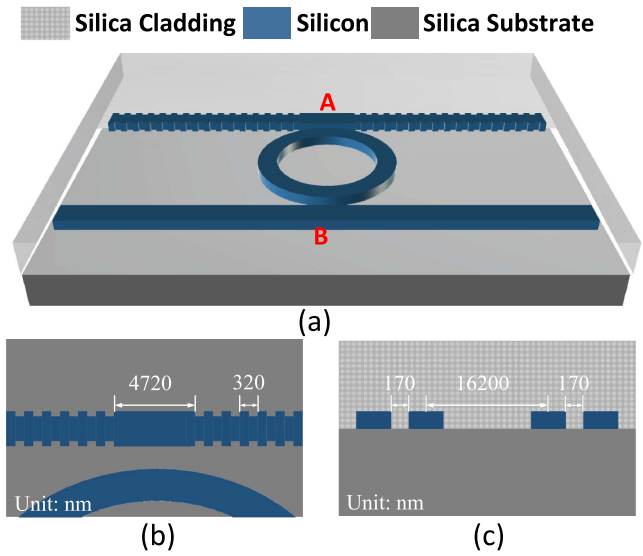

Fig. 1. (a) Perspective view of a grating-based FP cavity-coupled MRR. (b) Top view of the coupling region between the FP cavity and the MRR in (a). (c) Cross-sectional view of the planar along the direction from A to B on (a).

and the coupling gaps between the MRR and the two bus waveguides are designed to be 170 nm.

The transfer matrix method is used to simulate the transmission spectral response of the proposed device [17,18], and a typical simulation result is shown in Fig. 2(a). In the transmission spectrum, the grating-based FP cavity presents two wide dips, in the middle of which there is a resonance wavelength of the FP cavity, while the MRR presents four periodic narrow resonant dips. It is worth noting that one of the resonant wavelengths of the MRR is co-located with the resonance wavelength of the FP cavity, as indicated in the red dotted box in Fig. 2(a), which indicates that the two resonant modes are mutually coupled. Additionally, the relative position between the two resonance wavelengths indicates that this coupling is weak. Figure 2(b) shows a zoom-in view of the co-locating part, which exhibits an asymmetrical line shape. The coupling between the two resonant modes of the MRR and the FP cavity leads to a Fano resonance, and this coupling determines the line shape of the Fano resonance [10]. Moreover, this coupling could be adjusted by changing the relative position between the two resonant wavelengths or changing the coupling between the MRR and the FP cavity.

The device is fabricated using a CMOS-compatible technology with 193 nm deep ultraviolet lithography by IMEC,

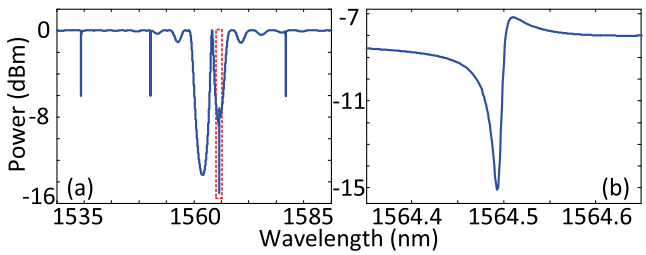

Fig. 2. (a) Simulated transmission spectral response of the proposed device. (b) Zoom-in view of the Fano resonance.

Belgium, accessed via ePIXfab. Figure 3(a) shows the layout schematic of the fabricated device obtained by a microscope camera. Four integrated waveguide-to-fiber grating couplers [19], placed uniformly on the chip with an identical space of 127 μm, are used to couple light into or out of the chip through an input and output fiber. Figure 3(b) shows a scanning electron microscope (SEM) image of the MRR. Figure 3(c) shows the fabricated gratings on the strip waveguide. Figures 3(d) and 3(e) show the coupling regions between the MRR and two bus waveguides. As can be seen, due to the fabrication imperfections, the designed square corrugations on the sidewalls show a sine-like shape after fabrication, which would lead to a wavelength drift of the Bragg wavelength.

The optical performance of the fabricated device is evaluated by using an optical vector analyzer (LUNA OVA CTe) to measure its transmission spectrum. Figure 4(a) shows the normalized spectral response at the pass port of the fabricated device. The insertion loss is estimated to be 13.65 dB, most of which comes from the low coupling efficiency of the grating coupler. Four periodic narrow dips with each having a full width at half-maximum (FWHM) of 0.085 nm, corresponding to a Q-factor of 18,000, are observed, which are the spectral response of the MRR. The free spectral range (FSR) of the MRR is about 11.3 nm. Two wide dips in the spectral response are observed, which are caused by the grating-based FP cavity. As can be seen, the resonance wavelength of the FP cavity is around 1554.7 nm with a FWHM of 0.490 nm, corresponding to a Q-factor of 3,200. More importantly, one of the resonance wavelengths of the MRR is co-located with the resonance wavelength of the FP cavity, as indicated by the red dotted box in Fig. 4(a), which indicates that there is a mutual coupling between the two resonant modes. Such a coupling would lead to a Fano resonance. Figure 4(b) shows a zoom-in view of the co-locating part, which exhibits an asymmetric line shape of a Fano resonance. The Fano resonance has an ER as large as 22.54 dB and an SR of 250.4 dB/nm, which is highly suitable for high-sensitivity sensing or low power optical switching/modulating. In addition, compared with the simulation results in Fig. 2, the measured spectrum of the fabricated device in Fig. 4 matches well with the simulated spectrum except the resonance wavelengths are slightly shifted, which is caused by the fabrication imperfections, and the line shape of the generated Fano resonance is slightly different, which resulted from the different coupling between the two resonant modes of the MRR and the FP cavity.

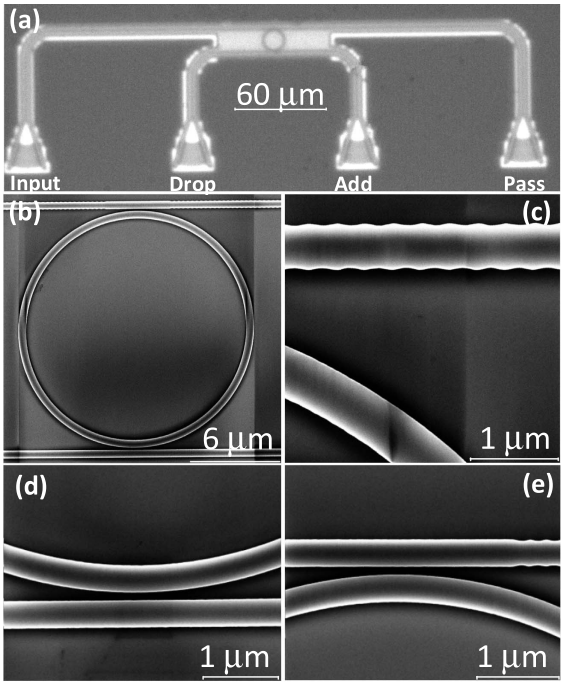

Fig. 3. (a) Image of the fabricated device layout obtained from a microscope camera, SEM image of (b) the fabricated MRR, (c) the Bragg gratings, (d) the coupling region near the drop port, and (d) the coupling region between the MRR and the FP cavity.

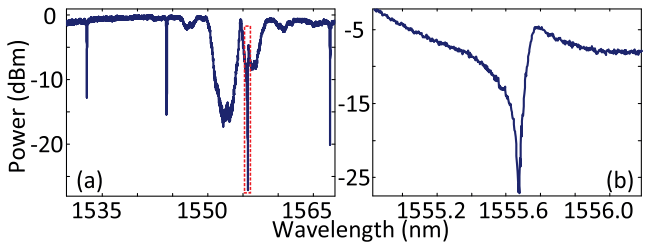

Fig. 4. (a) Normalized transmission spectral response at the through port of the fabricated device. (b) Zoom-in view of the Fano resonance of the fabricated device.

To further study the effect of the coupling between two resonant modes in the MRR and the FP cavity on the Fano resonance, a few more devices with different coupling gaps between the MRR and the FP cavity are fabricated. A numerical simulation is first made to study the effect, and Fig. 5(a) shows the simulation results. As can be seen, with the coupling coefficient between the MRR and the FP cavity varied, the Fano resonance is changed. This is because the Fano resonance is produced by the coupling between the resonant modes of the MRR and the cavity. When the coupling coefficient between the MRR and the FP cavity is changed, the coupling between the two resonant modes of the MRR and the FP cavity would be changed, which would lead the Fano resonance to be changed. In addition, as the coupling coefficient is decreased, the ER of the Fano resonance is decreased and the SR is increased, which is determined by the coupling condition between the MRR and the FP cavity. Figure 5(b) shows the measured Fano resonances of the fabricated devices with the coupling gap varied from 170 to 270 nm. As the coupling gap is increased, the coupling coefficient is decreased. It is clear in Fig. 5(b) that the ER of the measured Fano resonances becomes smaller and the SR becomes larger, which matches well with the simulation results in Fig. 5(a) except the resonance wavelength is slightly drifted, which is again caused by the fabrication imperfections, and the line shape of the generated Fano resonance is slightly different, which again resulted from the different coupling between the two resonant modes of the MRR and the FP cavity. This experimental result confirms that by changing the coupling between the MRR and the FP cavity, the Fano resonance could be changed.

To study all-optical tunability of the Fano resonance, we measure the Fano resonance when a pumping light with a wavelength at the resonance wavelength of either the MRR or the FP cavity is fed to the fabricated device from the input port. Thanks to the high Q-factor of the FP cavity and the MRR, their strong light-confinement capacity would strengthen the

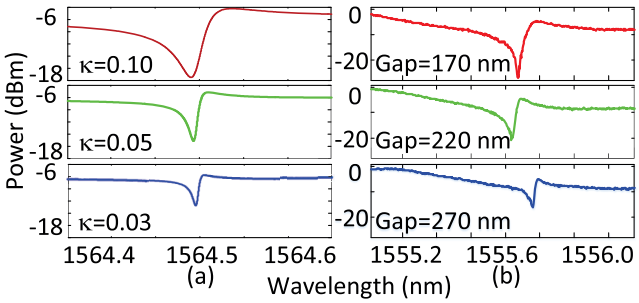

Fig. 5. (a) Numerical simulation result of the Fano resonance when the coupling coefficient is changed from 0.15 to 0.05. (b) Measured Fano resonance when the coupling gap is changed from 170 to 270 nm.

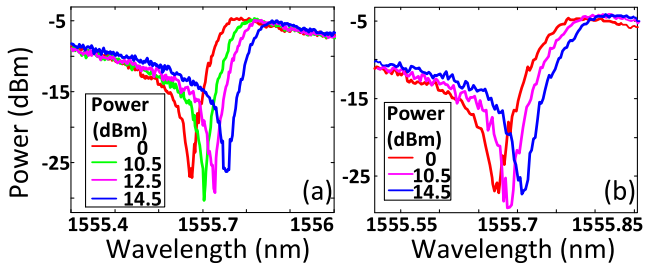

Fig. 6. Measured Fano resonance when a pumping light with a wavelength at the resonance wavelength of (a) the MRR and (b) the FP cavity is fed into the device.

TPA-induced nonlinear thermal-optic effect [20], which would finally affect the coupling between the MRR and the FP cavity. Therefore, by varying the power of the pumping light, the Fano resonance is tuned. To demonstrate the optical tunability, a pumping light with a wavelength of 1544.172 nm at the resonance wavelength of the MRR is first fed into the device. The pumping light is confined in the MRR, and the TPA-induced nonlinear thermal-optic effect would increase the refractive index of the silicon. Thus, the coupling between the FP cavity and the MRR is changed. The measured Fano resonance is shown in Fig. 6(a). As can be seen, as the power of the pumping light increases from 0 to 14.5 dBm, the Fano resonance is red-shifted, which confirms the all-optical tunability. The maximum tuning range is measured to be 90 pm when the power of the pumping light is increased to 14.5 dBm. Then, a pumping light with a wavelength of 1554.7 nm at the resonance wavelength of the FP cavity is fed into the device. The pumping light is confined in the FP cavity, and the TPA-induced nonlinear thermal-optic effect would increase the refractive index of the FP cavity. Thus, the coupling between the FP cavity and the MRR is affected. The measured Fano resonance is shown in Fig. 6(b). As can be seen, the Fano resonance is red-shifted by 20 pm when the power of the pumping light is 14.5 dBm, which again confirms the all-optical tunability. To improve the tuning range, two approaches of increasing the power of the pumping light or elevating the Q-factor of the two resonators could be used. Note that during the tuning, the ER and SR of the Fano resonance are also changed. This is because the TPA-induced nonlinear thermal-optic effect also affects the coupling condition between the MRR and the FP cavity. This device could find potential applications in ultrafast integrated photonic devices, such as all-optical switching, all-optical logic gates, and all-optical routers.

In summary, a grating-based FP cavity-coupled MRR on a silicon chip with an all-optically tunable Fano resonance was demonstrated. In the device, an add-drop MRR was employed and one of the two bus waveguides was replaced by an FP cavity consisting of two sidewall Bragg gratings as two reflectors. By carefully choosing the grating period and the FP cavity length, the resonant mode of the FP cavity was coupled to one of the resonant modes of the MRR. Due to the mutual coupling, a Fano resonance with an ER of 22.54 dB and an SR of 250.4 dB/nm was experimentally achieved. A further study of the effect of the coupling between the MRR and FP cavity on the Fano resonance was performed numerically and experimentally. Thanks to the strong light-confinement capacity of the MRR and the FP cavity, a strong TPA-induced nonlinear thermal-optic effect resulted, which was used to tune the Fano resonance optically. The key advantage of the proposed device is that the incorporation of the FP cavity in the MRR can maintain the compactness of the MRR and realize the optical tunability of the Fano resonance by using the high light-confining capacity of the two resonators.

Funding. Natural Sciences and Engineering Research Council of Canada (NSERC).

Acknowledgment. This work is supported by the Natural Sciences and Engineering Research Council of Canada (NSERC) under the Silicon Electronic-Photonic Integrated Circuits (Si-EPIC) CREATE program. We acknowledge CMC Microsystems for providing the design tools and enabling the fabrication.

REFERENCES

1. U. Fano, Phys. Rev. **124**, 1866 (1961).
2. B. Luk'yanchuk, N. I. Zheludev, S. A. Maier, N. J. Halas, P. Nordlander, H. Giessen, and C. T. Chong, Nat. Mater. **9**, 707 (2010).
3. R. Asadi, M. Malek-Mohammad, and S. Khorasani, Opt. Commun. **284**, 2230 (2011).
4. F. Cheng, H. F. Liu, B. H. Li, J. Han, H. Xiao, X. F. Han, C. Z. Gu, and X. G. Qiu, Appl. Phys. Lett. **100**, 131110 (2012).
5. H. C. Liu, C. Y. Song, Z. R. Wasilewski, J. A. Gupta, and M. Buchanan, Appl. Phys. Lett. **91**, 131121 (2007).
6. V. A. Fedotov, M. Rose, S. L. Prosvirnin, N. Papasimakis, and N. I. Zheludev, Phys. Rev. Lett. **99**, 147401 (2007).
7. F. Zhang, X. Y. Hu, Y. Zhu, Y. L. Fu, H. Yang, and Q. H. Gong, Appl. Phys. Lett. **102**, 181109 (2013).
8. M. Hochberg and T. Baehr-Jones, Nat. Photonics **4**, 492 (2010).
9. C. M. Chang and O. Solgaard, Opt. Express **21**, 27209 (2013).
10. T. Hu, P. Yu, C. Qiu, H. Qiu, F. Wang, M. Yang, X. Jiang, H. Yu, and J. Yang, Appl. Phys. Lett. **102**, 011112 (2013).
11. S. Fan, Appl. Phys. Lett. **80**, 908 (2002).
12. L. Y. Mario, S. Darmawan, and M. K. Chin, Opt. Express **14**, 12770 (2006).
13. Y. Lu, J. Yao, X. Li, and P. Wang, Opt. Lett. **30**, 3069 (2005).
14. L. Zhou and A. W. Poon, Opt. Lett. **32**, 781 (2007).
15. A. C. Ruege and R. M. Reano, J. Lightwave Technol. **28**, 2964 (2010).
16. Y. S. Kivshar, Opt. Express **16**, 22126 (2008).
17. W. Liang, L. Yang, J. K. S. Poon, Y. Huang, K. J. Vahala, and A. Yariv, Opt. Lett. **31**, 510 (2006).
18. T. Erdogan, J. Lightwave Technol. **15**, 1277 (1997).
19. W. Bogaerts, R. Baets, P. Dumon, V. Wiaux, S. Beckx, D. Taillaert, B. Luyssaert, J. V. Campenhout, P. Bienstman, and D. V. Thourhout, J. Lightwave Technol. **23**, 401 (2005).
20. Y. Liu and H. K. Tsang, Appl. Phys. Lett. **90**, 211105 (2007).